

## SECOND-ORDER BOUNDARY ELEMENT METHOD CALCULATIONS OF HYDRODYNAMIC INTERACTIONS BETWEEN PARTICLES IN CLOSE PROXIMITY

CHIU Y. CHAN\*, ANTONY N. BERIS\*† AND SURESH G. ADVANI‡

*\*Department of Chemical Engineering, ‡Department of Mechanical Engineering, Center for Composite Materials, University of Delaware, Newark, DE 19716, U.S.A.*

### SUMMARY

A second-order boundary element technique was developed to simulate the 3D hydrodynamic interactions between multiple particles of arbitrary shape. This paper reports the results of an extensive validation procedure aimed at demonstrating the convergence characteristics of the technique, especially in cases where the particles are in close proximity. The quadratic elements are superior to the lower-order elements in terms of accuracy, computer storage and CPU time required, thus resulting in a significant improvement in the overall computational efficiency. Superparametric discretization improves the accuracy over isoparametric discretization but lowers the convergence rate of the method. When the interparticle gap becomes very small (less than 1% of the particle radius), the numerical solution diverges owing to inaccurate determination of the element contributions in the gap region. An adaptive subdomain integration scheme was developed that dramatically improved the integration accuracy and provided convergent solutions for problems of very small gaps down to 0.01% of the particle diameter.

KEY WORDS Boundary element method Local mesh refinement Convergence Small interparticle gap Adaptive subdomain integration Superparametric

### INTRODUCTION

Particle suspensions play an important role in a wide variety of natural and man-made processes, e.g. flow of blood particles and proteins, pipeline transport of slurries, paper making, processing of ceramics and polymeric or ceramic composite materials, etc. The prediction of the structure and rheological properties of suspensions is thus of both theoretical and practical interest. One of the critical issues is the determination of the many-body hydrodynamic interactions. This is particularly important in many suspensions, such as those encountered in the processing of composite materials, where highly non-spherical particles are used. As an example, in injection moulding of fibre-filled polymers, high fibre aspect ratios (as high as 1000) and high concentrations (as high as 60 wt%) are often used to obtain improved mechanical properties.<sup>1,2</sup>

In view of the above-mentioned complexities, meaningful numerical simulations can only be developed based on three-dimensional hydrodynamic interactions around flexible fibres. However, a direct three-dimensional (volume) discretization of the partial differential fluid mechanics

---

† Author to whom all correspondence should be addressed.

equations poses severe restrictions on the complexities of the problems that can be realistically handled without sacrificing the accuracy. An alternative approach is offered by the boundary element method (BEM), which has the advantage of reducing the dimensionality of the numerical problem by one, albeit at the expense of taking into account only the linear viscous forces. The assumption of a linear problem is justified by the fact that under typical processing conditions the particle Reynolds number is very small, of the order of  $10^{-5}$ , and the inertia effect may be safely neglected.

In solving a 3D physical problem using the BEM, only 2D surfaces need to be discretized in the numerical solution. In addition to lowering the computational requirements, the dimensionality reduction allows for an easier description of complex geometries resulting from surface deformation. Finally, the BEM technique can be easily adapted to a parallel computer architecture, which has emerged as the computational framework of choice promising increases in capabilities orders of magnitude over the most powerful single-processor supercomputers.<sup>3</sup>

Although a considerable amount of work has been devoted to discussing the theoretical issues behind the application of the BEM,<sup>4,5</sup> relatively little attention has been paid to discussing the important numerical issues that arise in its implementation. In this first of a series of papers we present the development of a high-order BEM technique and a detailed investigation of its convergence characteristics. In the second paper a coupled BEM–finite element method technique will be described to accommodate cases exhibiting non-linear flow behaviour.

## PREVIOUS WORK

In the last decade there has been an increasing use of boundary element techniques to numerically study the hydrodynamics of suspensions. The relevant previous work is summarized below. Briefly, in the BEM the particle surface is discretized into elements and the variables of interest are approximated on the surface using piecewise continuous interpolation functions. Two basic mathematical formulations are employed leading to (a) Fredholm's integral equations of the first kind (FIE-1) and (b) Fredholm's integral equations of the second kind (FIE-2).

The use of FIE-1 to solve the Stokes flow problem was pioneered by Youngren and Acrivos,<sup>6</sup> who studied steady state flows past single arbitrary rigid prolate spheroids of aspect ratios ranging from 0.5 to 100. The steady state Stokes problem has been solved for multiparticle systems in various particle configurations by Tran-Cong and Phan-Thien<sup>7,8</sup> for aspect ratios up to 5. Ascoli *et al.*<sup>9</sup> studied the sphere–wall interaction. More recently the dynamic Stokes problem of particle–particle interactions was studied by Boyington and Soane<sup>10</sup> and Ingber<sup>11,12</sup> for aspect ratios up to 10. Also, Stoops and Leal<sup>13</sup> studied the dynamics of a sphere moving towards an advancing flow front.

The formulation of the Stokes problem using FIE-2 was originally proposed by Odqvist.<sup>14</sup> Until recently it did not gain popular use since the resulting system of integral equations depends on six linearly independent eigenfunction solutions, which in general are not known explicitly (see Reference 6 for a complete discussion). However, on the basis of the mathematical reformulation of Power and Miranda,<sup>15</sup> Karrila *et al.*<sup>16</sup> were able to study the steady flow past spheres using FIE-2 without recourse to the eigenfunctions.

Either of the two formulations requires solving a set of linear integral equations. In the BEM, since after discretization of the variables the resulting matrices are fully populated, the storage and solution of such matrices deserve special attention. If a low-order interpolation function is used, the number of elements has to be increased for a given accuracy. The size of the matrices will be increased so much that if a direct matrix solution is sought, the size of the problem is significantly limited. Indeed, owing to the use of the low-order (constant or linear) interpolation

functions to approximate the particle geometry, the studies mentioned above were able to study only relatively low particle aspect ratios (up to 10).

The formulation of the BEM using FIE-1 is straightforward since it directly involves physical variables such as the velocities and the tractions on the boundaries. However, the drawback is that the resulting system of equations is typically ill-conditioned, which makes the use of a direct matrix solver necessary. In contrast, FIE-2 results in a set of well-conditioned integral equations. Karrila *et al.*<sup>16</sup> showed that the conditioning number is kept low even upon mesh refinement and thus allows for an iterative solution of the matrices and reduces both the storage and computational time requirements. Power<sup>17</sup> showed that integral equations of the second kind yield a more stable solution. However, the major drawback for FIE-2 is that it involves not the physical variables but rather the density distributions, which might fluctuate widely for particles of irregular shapes.<sup>18</sup> The physical variables need then to be determined in a postprocessing step.

An important concern is that as the particle–particle or particle–wall gap becomes small, the accuracy of the integrals becomes poor to the point that the BEM solution does not converge on mesh refinement. Without suffering loss of convergence, the smallest gap that has been studied in the numerical simulation of hydrodynamic interactions of spheres was about 4% of the sphere diameter.<sup>9,12</sup> As a result, for cases of non-spherical particles or multiple spheres in close proximity, where no analytic solutions exist, there is no way to control the numerical error *a priori*. This can pose severe limitations in investigating the particle dynamics, especially in concentrated suspensions where the probability of particles being in very close proximity to each other is high. The difficulty of integral evaluation in problems of close proximity is also recognized in other fields, e.g. elastodynamic problems involving narrow cracks.<sup>19,20</sup> One approach there was to use an asymptotic expansion of the stress locally around the crack tip.<sup>21</sup> Very recently Voutsinas and Bergeles<sup>22</sup> and Georg<sup>23</sup> proposed an adaptive integration scheme similar to the one that we developed independently and report in this paper.

Another important issue is the significance of the approximation of the surface geometry compared to that of the variables in the formulation. In the finite element method it is well known that an equal-order (isoparametric) approximation gives the best error/numerical effort ratio.<sup>24</sup> In the BEM, in which the variables are explicitly dependent on the surface geometry, it is expected that a higher-order surface geometry (superparametric) approximation might be beneficial. Indeed, Ingber<sup>11</sup> and Aliabadi and Hall<sup>25</sup> found that a superparametric discretization provided more accurate numerical results than the isoparametric discretization. In Ingber's study he used a quadratic discretization of the geometry and a constant discretization of the variables.

## FORMULATION

The Stokes flow over a domain  $\Omega$  past an arbitrary particle with surface  $\Gamma$  is described by

$$\nabla \cdot \mathbf{u} = 0, \quad \mathbf{0} = -\nabla p + \mu \nabla^2 \mathbf{u}, \quad (1)$$

where  $\mathbf{u}$  is the velocity vector,  $p$  is the pressure and  $\mu$  is the viscosity. Note that only the pressure and viscous terms are retained in the momentum equations. As shown in Figure 1, there are in general two boundary conditions,

$$\mathbf{u} = \bar{\mathbf{u}} \quad \text{on } \Gamma_1, \quad \mathbf{q} = \bar{\mathbf{q}} \quad \text{on } \Gamma_2, \quad (2)$$

where  $\{q_j\} = [\sigma_{jk}] \{n_k\}$  is the traction on the particle surface,  $\sigma$  is the stress tensor and  $\mathbf{n}$  is the outward normal.

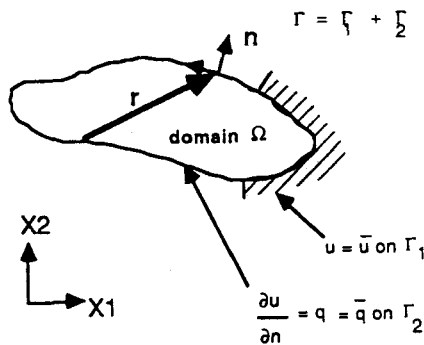


Figure 1. Boundary conditions for BEM formulation

The solution to the Stokes problem can be recast as the solution of a set of integral equations<sup>4</sup>

$$c^i u_j^i(\mathbf{x}) = \int_{\Gamma} u_{jk}^{i*}(\mathbf{x}, \zeta) q_k(\zeta) d\Gamma_{\zeta} + \int_{\Gamma} \sigma_{jkl}^{i*}(\mathbf{x}, \zeta) u_k(\zeta) n_l(\zeta) d\Gamma_{\zeta}, \tag{3}$$

where

$$c^i = \begin{cases} -1.0 & \text{if point 'i' is inside } \Omega \\ -0.5 & \text{if point 'i' is on } \Gamma \\ 0.0 & \text{if point 'i' is outside } \Omega \end{cases} \text{ for a smooth boundary.}$$

The functions  $u_{jk}^*$  and  $\sigma_{jkl}^*$  are the fundamental solutions or free space green functions and satisfy the governing equation (1). For flow in an unbounded domain they are given by<sup>26</sup>

$$u_{jk}^{i*} = \frac{1}{8\pi} \left( \frac{\delta_{jk}}{r} + \frac{r_j r_k}{r^3} \right), \tag{4}$$

$$\sigma_{jkl}^{i*} = \frac{1}{8\pi} \left( \frac{6r_j r_k r_l}{r^5} \right), \tag{5}$$

where  $r^2 = \mathbf{r} \cdot \mathbf{r}$  and  $\mathbf{r} = \mathbf{x} - \zeta$ . Physically,  $u_{jk}^{i*}$  represents the  $j$ th component of velocity at point  $\mathbf{x}$  due to a point force in the  $k$ -direction applied at  $\zeta$ . Equation (3) is written for each point of interest.

The pressure in the fluid is given by<sup>26</sup>

$$p = \int_{\Gamma} p_j^* q_j d\Gamma_{\zeta} + \int_{\Gamma} \phi_{jk}^* u_j n_k d\Gamma_{\zeta}, \tag{6}$$

where

$$p_j^* = \frac{1}{4\pi} \frac{r_j}{r^3}, \quad \phi_{jk}^* = \frac{1}{2\pi} \left( \frac{\delta_{jk}}{r^3} - \frac{3r_j r_k}{r^5} \right).$$

After the velocities and tractions are determined as the primary variables of the formulation, the pressure can be obtained as a secondary variable in a postprocessing step.

NUMERICAL IMPLEMENTATION

In the boundary element method the functions  $\mathbf{u}$  and  $\mathbf{q}$  are discretized and expressed as linear combinations of the interpolation functions  $\varphi_k$  weighted by the nodal values:

$$\mathbf{u}(\xi) = \sum_{k=1}^m \varphi_k \mathbf{u}_k, \quad \mathbf{q}(\xi) = \sum_{k=1}^m \varphi_k \mathbf{q}_k, \quad (7)$$

where  $\varphi_k$  is a piecewise continuous interpolation function and  $m$  depends on the order of the interpolation function and the type of element used (quadrilateral or triangular). In general the interpolation function can be of zeroth order (constant), first order (linear), second order (quadratic) or higher order. The higher-order functions will approximate the curvature of the variables better, thus improving the accuracy.<sup>27</sup> Similarly the domain geometry can be approximated as

$$\mathbf{x}(\xi) = \sum_{k=1}^m \Theta_k \mathbf{x}_k, \quad (8)$$

where  $\Theta_k$  is also a piecewise continuous interpolation function. If  $\varphi$  and  $\Theta$  are of the same order, the discretization is said to be 'isoparametric'. This has been found to give the optimal performance in the finite element method. However, for the BEM where the solution depends acutely on the approximation of the geometry, Aliabadi and Hall<sup>25</sup> have found that a superparametric discretization in which  $\Theta$  is of a higher order than  $\varphi$  is more advantageous.

In the collocation BEM the unknown nodal values are evaluated by solving a set of linear equations generated by writing equation (3) at each nodal point. At the  $i$ th nodal point, equation (3) in discretized form becomes

$$c^i \mathbf{u}^i = - \sum_{n=1}^N \int_{\Gamma_n} \mathbf{q} \mathbf{u}^{i*} d\Gamma + \sum_{n=1}^N \int_{\Gamma_n} \mathbf{u} \mathbf{q}^{i*} d\Gamma, \quad (9)$$

where  $N$  is the total number of elements in the problem. Equation (9) can be rearranged in the form

$$[\mathbf{H}_{ij}] \{u_j\} = [\mathbf{G}_{ij}] \{q_j\}, \quad (10)$$

where  $\mathbf{H}$  and  $\mathbf{G}$  are  $3M \times 3M$  influence matrices and  $\mathbf{u}$  and  $\mathbf{q}$  are the  $3M$  velocity and traction vectors on the boundary.  $M$  is the total number of nodes. Note that  $\mathbf{H}$  and  $\mathbf{G}$  depend only on the particle geometry and not on the boundary conditions.

For rigid particles the surface velocity is imposed as

$$\mathbf{u} = \mathbf{V} + \boldsymbol{\omega} \times (\mathbf{x} - \mathbf{x}_c), \quad (11)$$

where  $\mathbf{x}_c$  is the particle centre of mass. Equation (11) evaluated at the nodal points results in the vector equation

$$\{u_j\} = [\mathbf{A}_{jk}] \{(\mathbf{V}, \boldsymbol{\omega})_k\}, \quad (12)$$

where  $\mathbf{V}$  and  $\boldsymbol{\omega}$  are the translational and rotational velocity respectively and  $(\mathbf{V}, \boldsymbol{\omega})$  is a combined velocity vector.  $\mathbf{A}$  is a  $3M \times 6N_p$  matrix relating the particle velocities to the surface velocities, where  $N_p$  is the number of particles. The total force and total torque acting on a particle,  $\mathbf{F}^J$  and

$\mathbf{T}^J$  respectively, are given by

$$\mathbf{F}^J = \int_{\Gamma^J} \mathbf{q} \, d\Gamma, \quad (13)$$

$$\mathbf{T}^J = \int_{\Gamma^J} (\mathbf{x} - \mathbf{x}_c) \times \mathbf{q} \, d\Gamma, \quad (14)$$

where  $\Gamma^J$  is the surface of the  $J$ th particle.

### *Solution procedure*

There are in general two types of related problems. In the first type we are interested in evaluating the force and torque on the particles after specifying either the velocity or the traction. For problems of this type it is sufficient to first solve equation (10) alone and then evaluate the force and torque by a straightforward substitution of the velocities and tractions into equations (13) and (14).

The second type of problems involves specifying known forces and torques on the particle; both the velocity and traction are unknown. By combining equations (10), (11), (13) and (14), a new system of equations is obtained:

$$\left[ \begin{array}{c|c} [G_{ij}] & [-E_{ik}] \\ \hline [D_{kj}] & [0] \end{array} \right] \left\{ \begin{array}{c} \{q_j\} \\ \{(V, \omega)_k\} \end{array} \right\} = \left\{ \begin{array}{c} \{0\} \\ \{(F, T)_k\} \end{array} \right\}, \quad (15)$$

where  $\mathbf{E}$  is a  $3M \times 6N_p$  matrix equal to  $\mathbf{H}\mathbf{A}$ , with  $\mathbf{A}$  defined in equation (12),  $\mathbf{D}$  is a  $6N_p \times 3M$  matrix which is a function of surface area and connectivity,  $(\mathbf{F}, \mathbf{T})$  is a  $6N_p$  vector of force and torque components and  $(\mathbf{V}, \boldsymbol{\omega})$  is a  $6N_p$  vector of translational and rotational velocity components. The combined matrix on the left-hand side is the new influence matrix for the problem. Solution of equation (15) yields the desired tractions and velocities.

## NUMERICAL ISSUES

To fully realize the potential of the BEM, some critical issues on the implementation should be addressed since they limit the numerical efficiency and accuracy of the solution. These issues, although mentioned in the literature before, have not been addressed systematically. The objective of the work reported here is to develop a high-order BEM technique, convergent upon mesh refinement, that can accurately and efficiently handle three-dimensional flows around particles of arbitrary shape.

First, a systematic study of the effects of the discretization of the boundary as compared to that of the variables (isoparametric versus superparametric) is lacking. Also missing is the evaluation of the approximation error involved in the integrals and its effect on the convergence characteristics. Except in some very recent work,<sup>11,12</sup> most of the previous work used lower-order interpolation functions. For example, Karrila *et al.*<sup>16</sup> used 320 or more constant triangular elements to approximate the surface of a sphere. In our work a high-order (e.g. quadratic) interpolation function was used in conjunction with both isoparametric and superparametric discretization to efficiently approximate the arbitrary surface. The use of high-order interpolation functions offers the obvious advantage of higher accuracy, resulting in a minimization of the number of discrete variables, thus reducing the size of the matrices and permitting a direct matrix solution. However, no direct comparison has been reported.

Secondly, the solution to the Stokes problem involves integrations of singular functions. If a constant interpolation function is used, the singular integrations can be performed analytically.<sup>7,8,10,16</sup> However, for high-order interpolation functions and complex curved domains no analytical solution is available. Note that although the singular integrations are fewer in number than the non-singular integrations, the former usually affect the numerical accuracy more significantly. To calculate the singular integrals accurately, we used the methods of coordinate transformation and row sum.<sup>4,25</sup> In studying rigid body motion according to the row sum method, the sum of each row of the matrix **H** should add up to zero for unbounded flow and unity for bounded flow.

Thirdly, while the BEM has received much attention in the last decade and has been successfully applied to a wide variety of problems, the effort in developing error estimates has been relatively scarce.<sup>28-30</sup> Analytical results on the convergence of the BEM are only available for 2D problems and cannot be extended to three-dimensional cases.<sup>29</sup> Moreover, as the particle-particle or particle-wall gap becomes small, the accuracy becomes poor and often the solution does not converge. Without the loss of convergence the smallest gap that can be studied using FIE-1 was about 4% of the smallest characteristic dimension of the particles.<sup>9</sup> The issue is whether the poor convergence is caused by the above-mentioned ill-conditioning of the equations. Since particles may come very close to each other or to a wall, it is important to develop a more robust technique such that the error is maintained below certain ceiling values. A hybrid BEM-FEM technique based on the lubrication approximation in the gap region appears very promising and will be described in a later paper.<sup>31</sup>

The fourth critical issue is related to the computational efficiency. Since the matrix of the discretized integral equations is fully populated and each of the components is obtained from a sum of integrals, it is imperative to evaluate the integrals and to solve the resulting full matrix of equations efficiently. The computer codes were written in double-precision Fortran on an IBM 3090 vector computer. Gauss quadrature was used for the evaluation of the integrals. For triangular elements, product formulae were used to generate the Gauss points.<sup>32</sup> The matrix was solved directly using vector subroutines. An analysis showed that 90%–95% of the CPU time was spent on integrations, demonstrating the efficiency of the vectorized matrix solution routines.<sup>33</sup>

## RESULTS

We developed the high-order BEM and benchmarked it with the low-order methods in terms of accuracy, convergence, efficiency, storage and limitations. The eventual intent is to study the dynamics of particles of various complex geometries, in which case the error at each time step accumulates over time. Hence it is important to minimize the error for a given discretization.

The example problem of flow past rigid prolate spheroids in an unbounded domain was first considered in order to study the feasibility of the proposed BEM technique.<sup>34</sup> Test cases for both one- and two-particle systems were examined so that comparison with either analytic solutions<sup>35-39</sup> or the results of similar numerical studies<sup>7</sup> was possible. In discretizing the surface, triangular elements were used which allowed easy local mesh refinement at points where large gradients of stresses were anticipated. A typical mesh is shown in Figure 2. The particle aspect ratio ranged from 1 to 50.

For flow past a sphere in an unbounded domain Stokes' law is applicable and the drag force  $F_D$  is given by

$$F_D = 6\pi\mu Va, \quad (16)$$

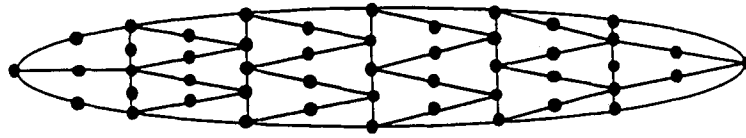


Figure 2. Typical mesh of a single prolate spheroid using triangular elements (six elements along major axis, four elements along minor axis; total 40 elements, 82 nodes)

where  $V$  is the far-field velocity and  $a$  is the sphere radius. For flow past a particle of arbitrary shape or past many particles a correction to Stokes' law is necessary:

$$F_D = 6\pi\mu Va_e R, \quad (17)$$

where  $a_e$  is the radius of a sphere with the same volume as the particle and  $R$  is the dimensionless drag ratio describing the effect of particle shape and particle-particle interactions. Similarly a dimensionless rotational velocity is defined as

$$\omega^* = \frac{\omega a}{V}. \quad (18)$$

#### Case 1. Flow past a single particle

First a detailed analysis of the effect of mesh refinement was performed using isoparametric discretization on flow past prolate spheroids.<sup>3,3</sup> The geometry (surface of the prolate spheroids) was represented by curved triangles mapped from the local  $(\eta_1, \eta_2)$  to the global  $(x, y, z)$  space using the same interpolation functions (biquadratic) as those used for the representation of the variables.<sup>4</sup> The convergence of the technique was studied using uniform mesh refinement in the case of a single prolate spheroid. As shown in Table I, the error in the drag ratio (and thus the translational velocity) decreased from 0.5% using the coarse mesh to less than 0.01% using the fine mesh. The case of flow past a single sphere was examined to demonstrate the numerical efficiency. As shown in Table II, this technique using 128 quadratic elements produced results that are of the same accuracy (about 0.02% error) as that of Karrila *et al.*<sup>16</sup> using 5120 constant elements.

The advantage of the high-order methods is apparent from Table III. For typical 3D problems using  $N_2$  quadratic elements the number of unknowns is roughly  $6N_2$ . The number of integrations required is about  $2(N_2)^2$  and the resulting full matrix is of size  $(6N_2)^2$ . Similarly, for  $N_0$  constant elements the number of unknowns is roughly  $3N_0$ ; the number of integrations required is about  $(N_0)^2$  and the resulting influence matrix is of size  $(3N_0)^2$ . Since for the same accuracy the value of  $N_0$  required is typically about  $40N_2$ , the constant elements required 800 times more integrations and 400 times more computer storage. Since over 90% of the CPU time is spent on evaluating integrals, the CPU time advantage for the quadratic elements is obvious despite the fact that the constant element integrations are computationally slightly less intensive. (In this comparison it is assumed that a direct matrix solution is used and thus all components are stored.) Also, since fewer unknowns are required, the condition number for the quadratic elements was only moderately high, thus allowing a stable direct matrix solution. Similar arguments apply to comparison between the quadratic and linear elements. Therefore the quadratic elements are superior to the lower-order elements in terms of accuracy, computer storage, CPU time required, conditioning of the influence matrix and thus the overall computational efficiency.



Table I. Drag ratio for one-prolate-spheroid cases using isoparametric discretization (uniform mesh refinement)

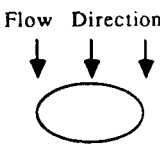
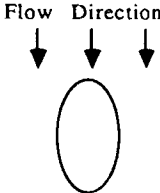
	Aspect ratio	No. of quadratic elements	Drag ratio	Error
	2	24	1.08910	-0.00533
		60	1.09365	-0.00078
		112	1.09433	-0.00010
		Exact	1.09433	
	2	24	0.95234	-0.00322
		60	0.95536	-0.00021
		112	0.95566	0.00009
		Exact	0.95557	

Table II. Drag ratio comparison for single-sphere case using isoparametric discretization: quadratic elements from this study versus linear elements from Reference 16 (uniform mesh refinement)

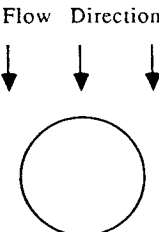
	Total no. of elements	Drag ratio	Error
	8 quadratic	1.02838	0.02838
	32 quadratic	1.00262	0.00262
	128 quadratic	1.00018	0.00018
	Exact	1.00000	
	320 constant	0.98082	-0.01918
	1280 constant	0.99726	-0.00274
	5120 constant	1.00033	0.00033

Table III. Constant versus quadratic elements

Constant element		quadratic element	
No. of elements	$N_0$	No. of elements	$N_2$
No. of unknowns	$M_0 = 3N_0$	No. of unknowns	$M_2 = 3(2N_2 + 2)$
No. of integrations	$N_0 \times M_0 / 3$	No. of integrations	$N_2 \times M_2 / 3$
Matrix size	$M_0 \times M_0$	Matrix size	$M_2 \times M_2$

For similar accuracy using a large number of elements:

$$N_2 = \frac{1}{40} N_0 \text{ is required}$$

$$\frac{\text{no. of integrations (constant)}}{\text{no. of integrations (quadratic)}} = \frac{N_0 \times M_0}{N_2 \times M_2} = 800$$

$$\frac{\text{storage (constant)}}{\text{storage (quadratic)}} = \frac{M_0 \times M_0}{M_2 \times M_2} = 400$$

Case 2. Flow past two particles—effect of local mesh refinement

For two-particle systems the results from this work agreed very well with previous BEM results by Tran-Cong and Phan-Thien<sup>7</sup> and asymptotic series results by Kim<sup>38</sup> within the number of significant figures that can be extracted from their graphical representations (see Table IV). Also studied was the case of flow past two nearly touching spheres, which is considered to be a numerically formidable task. As shown in Table V, the results from our technique converged reliably with an order of convergence equal to 3.6 and an error less than 0.02% using a moderately fine mesh of 128 elements. In contrast, the results of Tran-Cong and Phan-Thien<sup>7</sup> did not show a consistent convergence trend. In this paper the convergence order is defined with respect to an average element length (equivalent to an average nodal spacing  $\Delta h$ ).

Table IV. Drag ratio for two-prolate-spheroid cases using isoparametric discretization

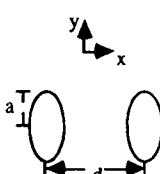
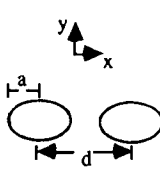
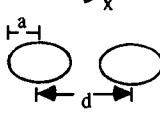
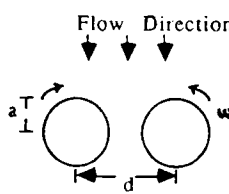
	Flow Direction	Particle aspect ratio	$d/a$	No. of elements	Drag ratio	
	z	2	4	24 quadratic	0.96548	
					80 linear <sup>7</sup>	0.96
		2	2	24 quadratic	0.86926	
					80 linear <sup>7</sup>	0.87
	y	2	3	24 quadratic	0.91799	
					60 quadratic	0.92106
					80 linear <sup>7</sup>	0.91
			x	2	4	24 quadratic
					60 quadratic	0.77861
					Asymptotic <sup>33</sup>	0.779
5	4			24 quadratic	0.91637	
				Asymptotic <sup>33</sup>	0.917	
			2	24 quadratic	0.80091	
				Asymptotic <sup>33</sup>	0.800	

Table V. Drag ratio comparison for flow past two nearly touching spheres with gap equal to 4.53% of diameter: quadratic elements from this study versus linear elements from Reference 8

	No. of elements per square	Drag ratio	Error
	8 quadratic	0.70289	-0.01482
	32 quadratic	0.71600	-0.00171
	128 quadratic	0.71759	-0.00012
	Exact	0.71771	
	80 constant	0.7224	0.0047
	128 constant	0.7241	0.0064
	192 constant	0.7214	0.0037

As shown in Table V, the relative error in the calculation of the rotational velocity was higher than for the translational velocity. Using a coarse mesh, the relative error on  $R$  was 2.1% and that on  $\omega^*$  was 6.2%; using a fine mesh, the relative error on  $R$  was reduced to 0.02% and that on  $\omega^*$  to 0.16%.

Mesh refinement was used to improve the numerical efficiency. Since high stresses exist in the interparticle or particle-wall gap, elements in the gap region were locally refined. Based on the uniformly spaced 32-element mesh, locally refined meshes of 48, 64 and 80 elements were generated. As shown in Table VI, using the 48-element locally refined mesh yielded the same accuracy as the 128-element uniform mesh but required only one-seventh of the CPU time. The refinement in this case was implemented *a priori* because of the known structure of the solution to the problem. In principle it can be implemented adaptively through an evaluation of the local error, which can be approximated, for example, through an evaluation of the magnitude of variation of the variables within an element. This issue will be discussed again in Case 6.

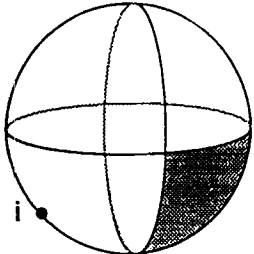
### Case 3. Superparametric BEM

Superparametric discretization was investigated as a means to improve the numerical accuracy. For particles of arbitrary shape superparametric discretization can be achieved by using a higher-order approximation to represent the geometry than to represent the velocity and traction variables. As an example a non-singular integration in an element was evaluated using various combinations of geometry and velocity approximations. For this test the geometry was taken to be one-eighth of a sphere (see the diagram in Table VII). The reported exact values were mesh-convergent results. As shown in Table VII, when the velocity was approximated quadratically, a third-order geometric approximation significantly improved the value of the integral over a second-order one. Using a fourth-order geometric discretization further improves the value. An asymptotic value was obtained when an exact representation of the geometry was used.

Table VI. Velocities for flow past two nearly touching spheres with gap equal to 4.53% of diameter using local mesh refinement. The eight-, 32- and 128-element meshes are uniformly refined whereas the 48-, 64- and 80-element meshes are locally refined based on the 32-element mesh

Discretization	No. of quadratic elements	Drag ratio	Error	Rational velocity	Error
Isoparametric	8	0.70289	-0.01482	0.10412	0.00606
	32	0.71600	-0.00171	0.10023	0.00217
	128	0.71759	-0.00012	0.09822	0.00016
	48	0.71658	-0.00013	0.09786	-0.00020
	64	0.71660	-0.00011	0.09765	-0.00041
	80	0.71660	-0.00011	0.09764	-0.00042
Superparametric	8	0.71747	-0.00024	0.10383	0.00577
	32	0.71760	-0.00011	0.10003	0.00197
	128	0.71769	-0.00002	0.09819	0.00013
	48	0.71768	-0.00003	0.09822	0.00016
	64	0.71770	-0.00001	0.09813	0.00007
	80	0.71770	-0.00001	0.09813	0.00007
Exact		0.71771		0.09806	

Table VII. Double-layer velocity components at point *i* due to motion of the shaded element for the problem in which gap is equal to 4.53% of diameter

	Order of velocity discretization	Order of geometric discretization	$u_1$	$u_2$	$u_3$	Comment
	2	1	2.571066	0.755311	0.484366	Subparametric
		2	3.769483	1.496275	0.319466	Isoparametric
		3	3.822645	1.518831	0.301669	Superparametric
		4	3.818758	1.517433	0.302715	Superparametric
		Exact	3.817712	1.518134	0.304701	Superparametric
	Exact	Exact	3.807015	1.513877	0.304556	

contribution of the shaded element (1/8 of the sphere) on the node

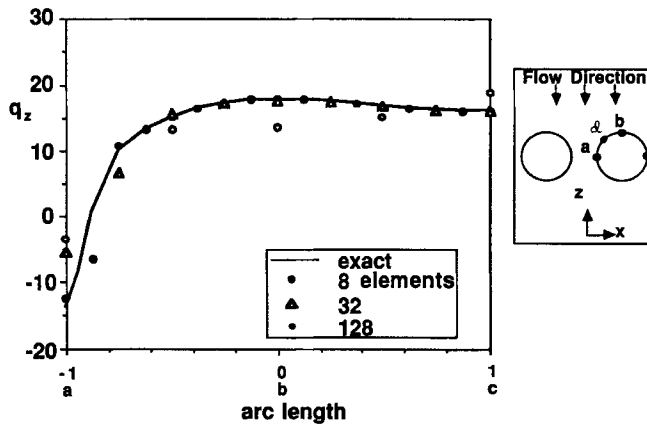


Figure 3(a). Z-component of traction along points 'a', 'b' and 'c' on plane parallel to flow direction using isoparametric discretization (gap equal to 4.53% of sphere diameter)

In the following test cases, in which only spheres were studied, superparametric discretization was implemented by using an exact representation of the geometry in terms of the spherical coordinates and a quadratic approximation of the velocity and traction variables. Each element was taken to be a spherical triangle, each edge of which is part of a great circle on the sphere's surface. The integration variables were the two solid angles, thus yielding a quadrilateral integration domain. As shown in Table VI, using 32 superparametric elements yielded the same accuracy on the drag ratio as using 128 isoparametric elements and required only one-fourth of the CPU time. However, the improvement was less dramatic with respect to the rotational velocity  $\omega^*$ .

As shown in Figure 3, the high-order BEM technique provides very accurate simulation of the tractions, which will be needed to determine local solid deformation of deformable particles. The exact traction was based on the series expansion expression of the velocity profile by Goldman

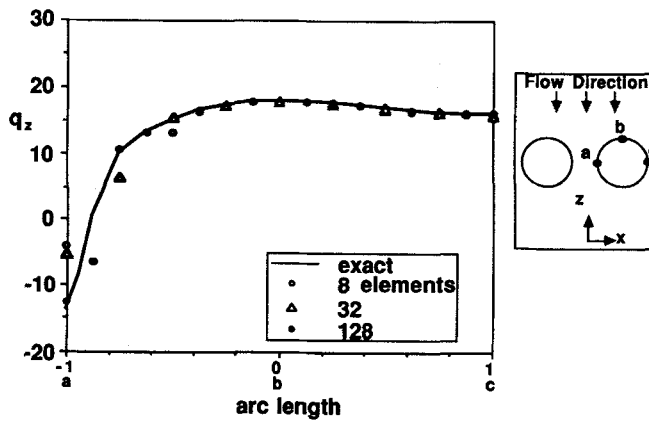


Figure 3(b). Z-component of traction along points 'a', 'b' and 'c' on plane parallel to flow direction using superparametric discretization (gap equal to 4.53% of sphere diameter)

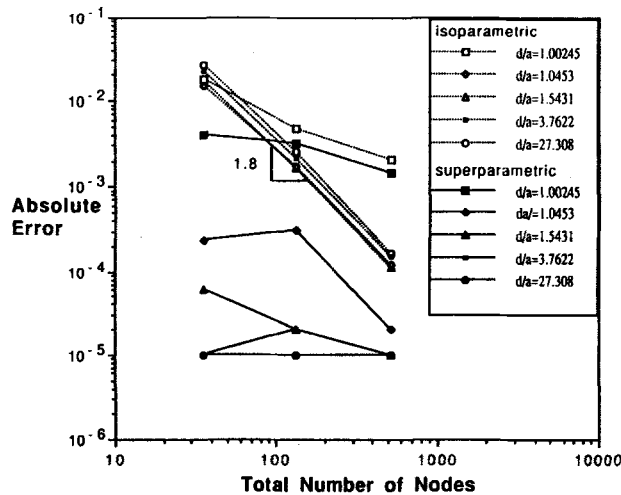


Figure 4(a). Error on drag ratio ( $R$ ) for flow past two spheres using isoparametric and superparametric elements

*et al.*<sup>39</sup> Note that the traction determined from the 32-element mesh matched the exact profile except in the gap region around the point of closest contact. Better accuracy in that region was achieved upon mesh refinement.

*Case 4. Convergence acceleration*

In Figure 4 the convergence rate with mesh refinement corresponding to the two discretization schemes is compared for the problem of flow past two spheres in which the centre-to-centre distance varies up to 27.308 diameters. The isoparametric elements showed a consistent convergence order of 3.6 for both  $R$  and  $\omega^*$ , independent of the gap size provided that the gap width was larger than about 1%. On the other hand, superparametric elements showed a convergence order of 1.6 for  $\omega^*$ , although the error obtained for a given discretization was consistently smaller than

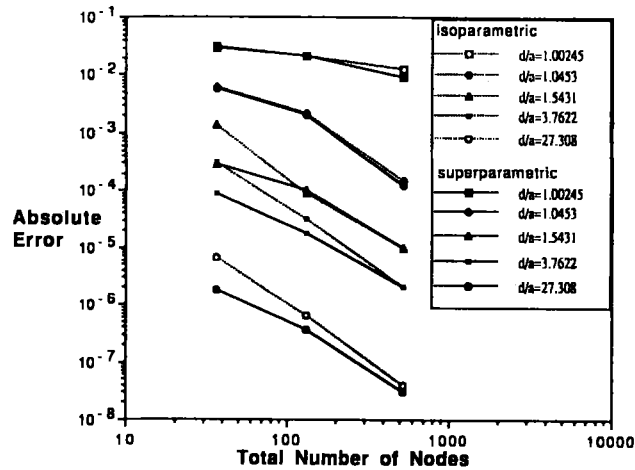


Figure 4(b) Error on rotational velocity ( $\omega^*$ ) for flow past two spheres using isoparametric and superparametric elements

that of the isoparametric elements. We interpreted the higher convergence order in the isoparametric case as a result of the greater sensitivity to the error in approximating the geometry. While we did not carry out further mesh refinement, it is intuitive that as we refine the mesh further, the error due to the geometric representation from the isoparametric discretization will decrease and asymptotically approach that from the superparametric discretization. Therefore we speculate that if the mesh refinement process is extended beyond the current range, the convergence order from the isoparametric discretization will decrease and asymptotically approach that from the superparametric discretization and that the error in the solution from the isoparametric discretization will always be higher than that from the superparametric discretization.

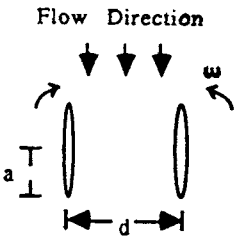
The power and benefits of a convergent numerical method are that the accuracy of the numerical result can be improved using standard convergence acceleration techniques such as the Shanks, transformation.<sup>40</sup> For the case of flow past prolate spheroid of aspect ratio 50, the uniformly refined meshes yielded errors on  $R$  of 1.0%, 0.36% and 0.27% respectively. The Shanks transformation (without additional computation) based on these three results reduced the error to 0.09% (see Table VIII). Thus, instead of using a finer mesh which demands much higher CPU time and computer storage, using the convergence acceleration technique yields a substantially more accurate solution.

#### Case 5. Cause of divergence in solutions to close proximity situations

As shown in Figure 4, the convergence of the high-order BEM technique became worse as the particle gap decreased to below 1% of the particle diameter, irrespective of the discretization used. In some cases the solution diverged upon mesh refinement. The poor accuracy was particularly evident for the traction in the gap region, which was poorly determined and in some cases even with the wrong sign. We undertook a rigorous and systematic study of the causes for this divergence in which we investigated the errors associated with specific steps in the BEM procedure. The results of this study are briefly outlined below.

- (a) The singular integration was separately performed using  $n \times n$  Gauss points, where  $n$  is in the range 6–20. Note that in using the spherical co-ordinate system to describe the surface of spheres exactly, the two solid angles become the integration variables. The singularities

Table VIII. Convergence acceleration using the Shanks transformation (uniform mesh refinement). For the mesh the first number is the number of elements along the major axis and the second number is the number of elements along the minor axis

	Aspect ratio	Total no. of ellipsoids	Mesh used	Drag ratio	Error	
	2	1	4 × 4	0.95234	-0.00324	
			5 × 5	0.95473	-0.00085	
			6 × 6	0.95536	-0.99922	
			Shanks	0.95558	0.00001	
			Exact	0.95557		
		2	4 × 4	0.72139		
			5 × 5	0.72286		
			6 × 6	0.72326		
			Shanks	0.72341		
			10 × 10	0.72342		
		50	1	12 × 4	2.181	-0.022
				15 × 5	2.211	0.008
				18 × 6	2.197	-0.006
				Shanks	2.201	-0.002
Exact	2.203					
2	4 × 4		1.504			
	15 × 5		1.518			
	18 × 6		1.511			
	Shanks		1.513			

due to  $u_{ij}^*$  and  $\sigma_{ijk}^*$  are cancelled and there is no need for special integration. It was found that the value of  $\int_{\Gamma} u_{ij}^* q_j d\Gamma_{\zeta}$  converged to within  $10^{-7}$  of the exact solution using only  $6 \times 6$  Gauss points. The integral  $\int_{\Gamma} \sigma_{ijk}^* u_j n_k d\Gamma_{\zeta}$ , normally conceived as singular, was found to behave as weakly singular and converged to within  $10^{-7}$  of the exact solution using  $10 \times 10$  Gauss points. Hence the row sum method was not needed to determine the diagonal components of the matrix **H**. It will be used as a check on the accuracy with which the integral contributions are evaluated (see below).

- (b) To determine the influence of error accumulation in the solution of the linear equations, the condition number of the resulting matrix was monitored as a function of the discretization. The condition number was calculated as  $\| \mathbf{G} \|_{\infty} \times \| \mathbf{G}^{-1} \|_{\infty}$ , the infinite norm of the matrix and its inverse.<sup>34</sup> As shown in Figure 5, the condition number increased with the number of elements to the power of approximately 2.5 for gaps larger than 1% of the sphere diameter. Below that the condition number increased erratically. Although the largest condition number encountered was of the order of  $10^9$ , it did not affect the solution accuracy directly. The reason for this unexpected behaviour is explained below.
- (c) The matrix is normally stored and solved in double precision using the highly efficient, vectorized double-precision ESSL subroutines (DGEF and DGES) in an IBM 3090 environment. In order to ascertain the effect of the high condition number on the accuracy of the solution, a Gaussian elimination subroutine in quadruple precision was used. In all cases tested it was found that the quadruple- and double-precision results agree with each other within  $10^{-10}$  despite the high condition number.
- (d) The non-singular integration was evaluated using  $n \times n$  Gauss points, where  $n=6-20$ . It was found that while the value of most integrals converged using as few as  $4 \times 4$  Gauss

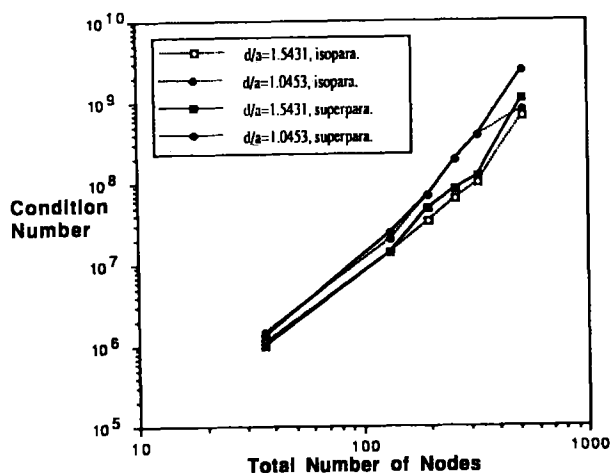


Figure 5. Condition number of influence matrix

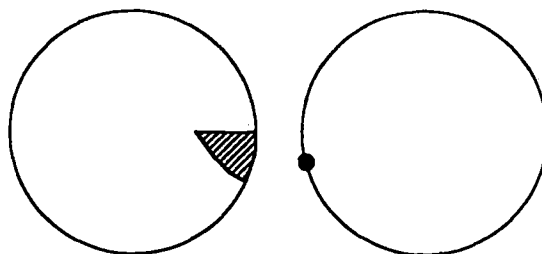


Figure 6. Contribution of element in gap region to collocation point on neighbouring sphere

points, there existed a few integrals for which the values did not show any trend of convergence. Specifically these were integrals which involve elements in the gap (see Figure 6). Moreover, the values of these integrals were at least an order of magnitude larger than the rest of the integrals. Even a slight error in their determination had a magnified effect on the diagonal components of the matrix  $\mathbf{H}$  as obtained using the row sum method.

Hence it was concluded that as the interparticle gap decreased, the error accumulation resulted from the inaccuracy in determining the disproportionately large, nearly singular contributions to the influence matrix from the elements in the gap region.<sup>31</sup>

#### Case 6. Adaptive subdomain integration

An adaptive subinterval integration was developed to improve the integration accuracy. The domain was subdivided into subdomains, with the length of the subdomain halved during each subdivision (see Figure 7). The process of subdivision was continued until the sum of the subdomains agreed with the parent domain within a convergence criterion (typically  $10^{-10}$  of the normalized sum of the components in a row). Similar ideas on domain subdivision have been proposed and demonstrated by Voutsinas and Bergeles<sup>22</sup> and Georg.<sup>23</sup>

With the inaccuracies in the integration procedure removed, all components of matrices  $\mathbf{H}$  and  $\mathbf{G}$  can be obtained accurately through a direct evaluation of the integrals without recourse to



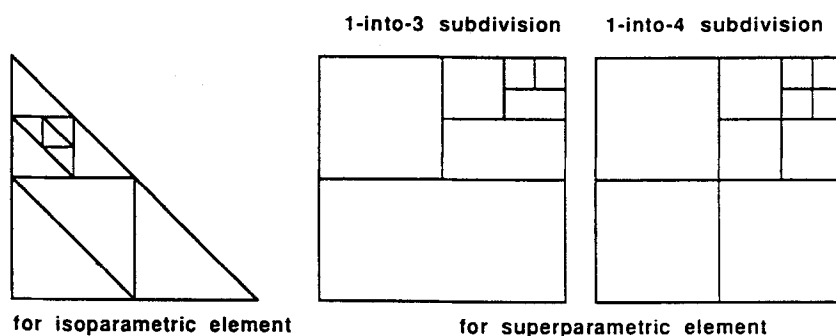


Figure 7. Adaptive sub-domain integration

using the row sum method. This allowed us to use the row sum as an independent check on the accuracy of the integrations. From our experience, for the isoparametric elements which have a triangular integration domain, triangular subdivision proves to be the most efficient and straightforward. For the superparametric elements which have a quadrilateral integration domain, a one-into-three subdivision scheme is more efficient than a one-into-four scheme (see Figure 7). For the elements outside the gap, usually no subdivision is required. For the elements in the gap, seven to 11 levels of subdivisions were required for gaps smaller than 1% of the particle diameter.

As shown in Table IX, the range of convergence was extended to very small particle diameters less than 0.01% of the sphere diameter. Note that in the case of a 0.01% gap the side of the smallest element in the 80-element mesh is 980 times larger than that of the gap width. While very small gaps are not likely in the cases of spheres owing to the development of large hydrodynamic lubrication forces, it is possible for small gaps to develop locally along fibres.

A few additional notes should be made.

- (a) The condition number was influenced mostly by the size of the problem. This shows the advantage of using a higher-order approximation and local adaptive mesh refinement geared towards reducing the number of elements required for a given accuracy. There was only a minor effect of particle gap size on the condition number. Overall the condition number increased with the number of elements to the power of 2.5, which is consistent with the observation in Case 5 above.

In the absence of sub-domain integration the condition number was higher for the same size of problem owing to errors in the matrix components (compare Figure 5 with Figure 8). As an example, in using the 80-superparametric-element mesh to solve the problem of flow past two spheres in which the gap was 0.245%, the condition number was  $1.8 \times 10^8$  using sub-domain integration and  $2.9 \times 10^{12}$  if subdomain integration was not used.

- (b) A Gaussian elimination subroutine in quadruple precision was used to check the error in solving the matrix resulting from using subdomain integration. In two cases tested (the 216- and 256-element meshes) it was again found that the quadruple- and double-precision results agree with each other within  $10^{-10}$  despite the moderately high condition numbers ( $1.1 \times 10^9$  and  $4.6 \times 10^9$ ).
- (c) For locally refined meshes the results showed a trend of monotonic convergence up to the 64-element mesh. Further local refinement to the 80-element mesh yielded errors with the opposite sign. Indeed, the 96-element mesh yielded worse results than the 80-element mesh. We further checked the effectiveness of local refinement by using two additional meshes: the

Table IX. Results for flow past two nearly touching spheres using superparametric elements (see Figure 3(a) for location of point 'd')

Gap/diameter	Number of quadratic elements	Condition number	Drag ratio	Rotational velocity	Traction at point 'd'
0.0100	8	$4.8 \times 10^5$	0.71044	0.10807	12.977
	32	$1.8 \times 10^7$	0.71107	0.09806	16.348
	128				
	48	$2.6 \times 10^7$	0.71225	0.09046	15.488
	64	$4.6 \times 10^7$	0.71262	0.08815	15.265
	80	$8.4 \times 10^7$	0.71264	0.08804	15.258
	Exact		0.71264	0.08793	14.995
0.00245	8	$8.0 \times 10^5$	0.70891	0.10851	12.906
	32	$3.6 \times 10^7$	0.70977	0.09706	16.670
	128				
	48	$3.5 \times 10^7$	0.71153	0.08582	15.543
	64	$5.0 \times 10^7$	0.71271	0.07844	14.958
	80	$1.8 \times 10^8$	0.71296	0.07687	14.839
	Exact		0.71291	0.07717	14.580
0.0005	8	$9.4 \times 10^5$	0.70857	0.10855	13.068
	32	$3.6 \times 10^7$	0.70943	0.09684	16.844
	48	$4.1 \times 10^7$	0.71142	0.08415	15.553
	64	$8.2 \times 10^7$	0.71325	0.07267	14.714
	80	$5.6 \times 10^9$	0.71472	0.06337	14.121
		Exact		0.71414	0.06708
0.0001	8	$9.2 \times 10^5$	0.70823	0.10885	14.237
	32	$3.7 \times 10^7$	0.70952	0.09582	16.632
	128	$3.7 \times 10^9$	0.71139	0.08375	15.625
	48	$5.3 \times 10^7$	0.71142	0.08369	15.553
	64	$1.4 \times 10^8$	0.71340	0.07116	14.646
	80	$1.0 \times 10^9$	0.71606	0.05437	13.615
	96	$8.7 \times 10^{10}$	0.72422	0.02768	10.532
	216*	$1.1 \times 10^9$	0.71593	0.05533	13.439
	256†	$4.6 \times 10^9$	0.71579	0.05614	13.484
		Exact		0.71533	0.05908

\* Non-uniformly refined from the 64-element mesh.

† Uniformly refined from the 64-element mesh.

216-element mesh refined from the 64-element mesh was a non-uniformly refined mesh but the area of refinement covered a larger surface than the 80-element mesh; the 256-element mesh was a uniformly refined mesh. In terms of accuracy the 256-element mesh performed the best and the 216-element mesh performed better than the 80-element mesh. Hence there is a limit on the number of levels to which local mesh refinement can be carried out (see Table IX). In the light of these results the mesh refinement used in Case 2 was unnecessary and the major effect of mesh refinement was to locally reduce the quadrature error.

- (d) Finally, with all the techniques developed in this work (superparametric discretization and subdomain integration) and upon a uniform mesh refinement (over triangular elements with quadratic approximation of the variables) the convergence rate was found to be quadratic with element length in calculation of both the translational and rotational

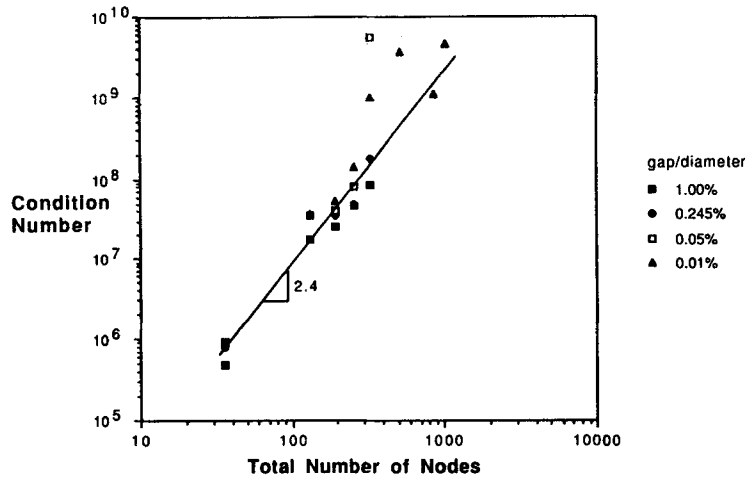


Figure 8. Condition number of influence matrix using superparametric elements and subdomain integration

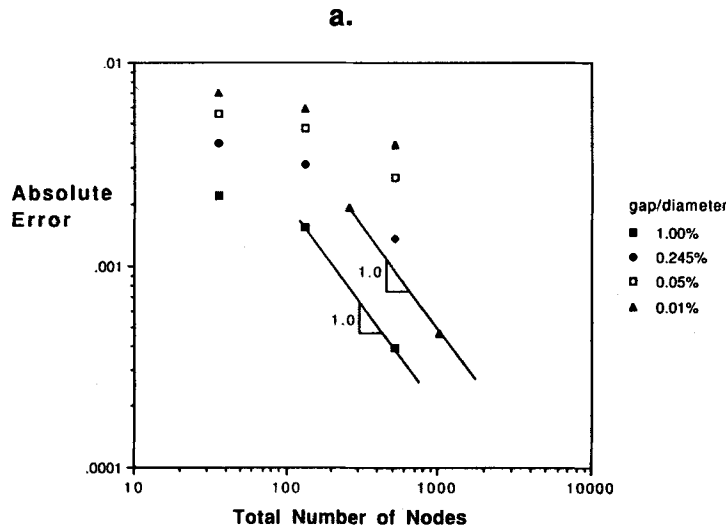


Figure 9(a). Error on drag ratio ( $R$ ) for flow past two spheres using superparametric elements and subdomain integration

velocities. In previous work which did not employ subdomain integration<sup>7,33</sup> the rotational velocity had poorer convergence than the translational velocity (for example, compare results for superparametric elements in Figures 4(a) and 4(b) with Figures 9(a) and 9(b). Note that results from the eight-element mesh were not used in determining the convergence order since the mesh is too coarse.

The local traction in general shows a linear convergence with respect to the element length (see Figure 10), which is in agreement with the quadratic convergence of the integral quantities (translational and rotational velocities). The convergence order decreases as the gap size decreases and as the closest point of contact is approached. Note that the local

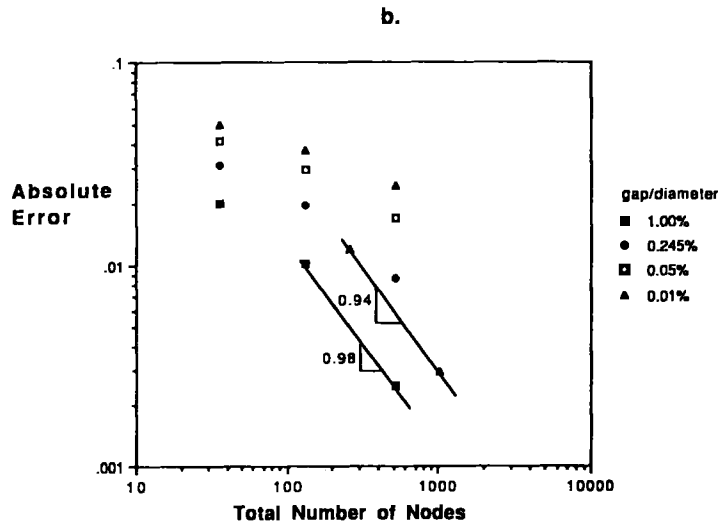


Figure 9(b). Error on rotational velocity ( $\omega^*$ ) for flow past two spheres using superparametric elements and subdomain integration

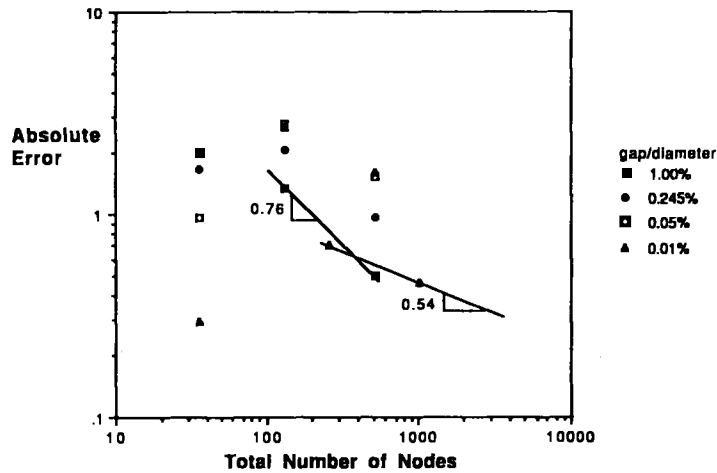


Figure 10. Error on traction at point 'd' of Figure 3(a) for flow past two spheres using superparametric elements and subdomain integration

traction has seldom been reported in previous work. It is the first time that robust convergence on local variables has been demonstrated.

- (e) Subdomain integration provides naturally a means for mesh refinement. As the domain is subdivided, the sum of the contributions from the subdomains is checked against that from the parent domain. If excessive subdivisions are required, indicating large variations in one or more of the variables, mesh refinement is recommended.

As mentioned before, theoretical results for convergence of the 3D collocation BEM are not available. Only results for the Galerkin and collocation BEM in 2D have been reported.<sup>28</sup> This seems to indicate that more work is necessary to address this important issue.

Case 7. Two opposing spheroids

To demonstrate the powerfulness of the adaptive subdomain integration scheme, the case of unbounded flow past two oblate spheroids (aspect ratio of 10) was studied. Oblate spheroids are used often to approximate discs. For the case of flow past a single oblate spheroid the results converged at an order of 5.1 (Table X). For the case of two oblate spheroids, opposing unit forces were imposed to push them towards each other. This problem is challenging since much of the surface is almost flat, which provides a large number of elements in close proximity to each other for cases of small gaps. Since there is no theoretical values for the drag ratio, we compare our far-field (large-gap) results with those of Yoon and Kim<sup>41</sup> and our near-field (small-gap) results with the asymptotic values of Cox.<sup>42</sup>

As shown in Table XI, our results for moderate gap sizes agree very well with the asymptotic values. In the range over which the asymptotic results are valid the typical errors are less than 1%, which is considerably better than those obtained by Yoon and Kim.<sup>41</sup> For small gaps a Shanks transformation was performed using the individual drag ratios determined from three meshes. The results were higher than the asymptotic value since it is well known that the small-gap asymptotic expansion result is valid over an extremely small range. Nevertheless, the trend of decreasing velocities (as indicated by increasing drag ratio values) as the gap narrows is captured very well. Also, the ratio of the Shanks-transformed results and the asymptotic values appears to decrease as the gap narrows.

DISCUSSION

The major contribution of this work is to show that the conventional boundary element technique (i.e. utilizing integral equations of the first kind) can be used to obtain accurate results that are mesh-convergent in Stokes flow problems. The numerical issues that need to be efficiently resolved to achieve accurate results involve higher-order interpolation functions, a superparametric evaluation of surfaces, adaptive mesh refinement and, most importantly, control of quadrature errors through successive subdomain integration. The second contribution is to demonstrate convergence not only for global quantities (such as the drag ratio) but also for local ones, in particular the traction, which can exhibit wide variations in regions where two surfaces are very close to each other.

It is rather difficult to explain the different convergence rates observed in this work mainly because of the absence of any mathematical theory for 3D problems. We can, however, speculate on some of the factors that influence the solution accuracy. Due to the high condition numbers, the errors in the solution might simply reflect the quadrature error in evaluating the integrals which constitute the components of the matrices **G** and **H**. In the superparametric cases, although

Table X. Drag ratio for one-oblate-spheroid case using isoparametric discretization with subdomain integration (uniform mesh refinement)

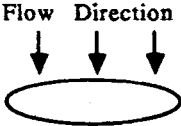
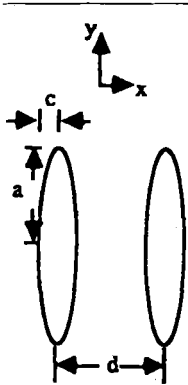
	Aspect ratio	No. of quadratic elements	Drag ratio	Error
	10	24	0.81734	-0.03511
		60	0.84410	-0.00835
		112	0.85146	-0.00099
		Exact	0.85245	

Table XI. Drag ratio for case of opposing unit force in  $x$ -direction acting on two oblate spheroids (aspect ratio  $c/a=10$ ) using isoparametric discretization with subdomain integration

	$(d-2c)/a$	No. of elements	Drag ratio
	4	24 quadratic	2.4624
		60 quadratic	2.5430
		Asymptotic <sup>42</sup>	2.5722
		YK <sup>42</sup>	2.63
	3	24 quadratic	2.7545
		60 quadratic	2.8433
		Asymptotic <sup>42</sup>	2.8795
		YK <sup>42</sup>	3.03
	2	24 quadratic	3.4189
		60 quadratic	3.5242
		Asymptotic <sup>42</sup>	3.5968
		YK <sup>42</sup>	4.67
0.8	24 quadratic	7.7900	
	60 quadratic	7.9917	
	YK <sup>42</sup>	21.6	
0.3	24 quadratic	32.662	
	60 quadratic	34.407	
	YK <sup>42</sup>	57.6	
0.05	24 quadratic	189.68	
	60 quadratic	533.33	
	112 quadratic	745.54	
	Shanks	1088	
0.025	Asymptotic <sup>43</sup>	2160	
	24 quadratic	113.82	
	60 quadratic	740.14	
	112 quadratic	1521.6	
	180 quadratic	2020.4	
Shanks	2901		
Asymptotic <sup>43</sup>	4317		

we have used an adaptive subdomain integration in order to keep the quadrature error always below the same bound, it is not clear if we have completely eliminated the influence of quadrature errors on the final solution. Furthermore, as the gap narrows, the traction function becomes so steep that we do not think that we have reached the asymptotic region on the convergence plot. Hence a hybrid approach may be appropriate for such cases. Finally, in the study of the flow around a single sphere or spheroid the very good convergence rates might be due to the exceptionally well-behaved solution for that problem.<sup>43</sup>

## CONCLUSIONS

In this paper a detailed convergence investigation of a quadratic BEM technique applied to 3D test flow problems was presented. The high-order technique, when implemented in an efficient and accurate fashion, yields mesh-convergent results even for problems of close proximity. Here, in the problems examined—flow past two almost touching spheres (with gap widths of the order of 0.1% of the sphere diameter)—64 elements per sphere was found to be adequate to yield errors

below 0.2%. The quadratic elements were found to be superior to the lower-order elements in terms of accuracy, computer storage, CPU time required, conditioning of the influence matrix and thus overall computational efficiency. The techniques of superparametric discretization and local mesh refinement were shown to improve the numerical efficiency dramatically. The poor convergence in cases of small particle gaps was caused by inaccurate determination of the disproportionately large contribution from elements in the gap region. An adaptive subdomain integration scheme was developed to improve the integration accuracy. The range of convergence in the test cases was extended to very small particle gaps down to 0.01% of the particle diameter. It was demonstrated that a convergent solution can be obtained using integral equations of the first kind despite a moderately high condition number. Clearly the same subdomain integration technique can be applied in the study of other fields, e.g. elastodynamics.

#### ACKNOWLEDGEMENTS

The authors gratefully acknowledge financial support of their research from the Center for Composite Materials at the University of Delaware and computational support from the Academic Computing Service at UD. They would also like to acknowledge stimulating discussion with Dr. Wendland who pointed out the significance of errors associated with integral contributions from elements in the gap.

#### REFERENCES

1. J. M. Crosby and T. R. Drye, 'Fracture studies of discontinuous fiber reinforced thermoplastic composites', *J. Reinf. Plast. Compos.*, **6**, 162-177 (1987).
2. S. Ward and J. Crosby, 'The influence of microstructure on the mechanical property performance of long fiber reinforced thermoplastic composites', *ANTEC'89 Proceedings Conference*, SPE, New York, 1989, pp. 1508-1512.
3. N. P. Smith (ed.), 'News and analysis', *Supercomputing Review*, **4** (12), 12-22 (1991).
4. C. A. Brebbia and J. Dominguez, *Boundary Elements: An Introductory Course*, McGraw-Hill, New York, 1988.
5. S. Kim and S. J. Karrila, *Microhydrodynamics: Principles and Selected Applications*, Butterworth/Heinemann, Boston, 1991.
6. G. K. Youngren and A. Acrivos, 'Stokes flow past a particle of arbitrary shape: a numerical method of solution', *J. Fluid Mech.*, **69**, 377-403 (1975).
7. T. Tran-Cong and N. Phan-Thien, 'Stokes problems of multiparticle systems: a numerical method for arbitrary flows', *Phys., Fluids A*, **1**, 453-461 (1989).
8. T. Tran-Cong, N. Phan-Thien and A. L. Graham, 'Stokes problems of multiparticle systems: periodic arrays', *Phys. Fluids A*, **2**, 666-673 (1990).
9. E. P. Ascoli, D. S. Dandy and L. G. Leal, 'Low Reynolds number hydrodynamic interaction of a solid particle with a planar wall', *Int. j. numer. methods fluids*, **9**, 651-688 (1989).
10. D. R. Boyington and D. S. Soane, 'Dynamic simulation of suspensions of non-spherical particles by boundary element technique', *Int. Polym. Proc.*, **4**, 35-43 (1989).
11. M. S. Ingber, 'Numerical simulation of the hydrodynamic interaction between a sedimenting particle and a neutrally buoyant particle', *Int. j. numer. methods fluids*, **9**, 263-273 (1989).
12. M. S. Ingber, 'Dynamic simulation of the hydrodynamic interaction among immersed particles in Stokes flow', *Int. j. numer. methods fluids*, **10**, 791-809 (1990).
13. J. A. Stoos and L. G. Leal, 'Particle motion in axisymmetric stagnation flow toward an interface', *AIChE J.*, **35**, 196-212 (1989).
14. F. K. G. Odqvist, 'On the boundary value problems in hydrodynamics of viscous fluids', *Math. Z.*, **32**, 327-375 (1930).
15. H. Power and G. Miranda, 'Second kind integral equation formulation of Stokes flow past a particle of arbitrary shape', *J. Appl. Math.*, **47**, 689-698 (1987).
16. S. J. Karrila, Y. O. Fuentes and S. Kim, 'Parallel computational strategies for hydrodynamic interactions between rigid particles of arbitrary shape in a viscous fluid', *J. Rheol.*, **33**, 913-947 (1989).
17. H. Power, 'Numerical methods for solving the low Reynolds number flow past a particle of arbitrary shape: a comparison work', in S. Grilli, C. A. Brabbia and A. H.-D. Cheng (eds), *Proc. Fifth Int. Conf. on Boundary Element Technology*, Springer New York 1990, pp. 253-262.
18. S. J. Karrila and S. Kim, 'Integral equation of the second kind for Stokes flow: direct solution for physical variables and removal of inherent accuracy limitation', *Chem. Eng. Commun.*, **82**, 123-161 (1989).
19. T. A. Cruse, 'Fracture mechanics', in *Boundary Element Methods in Mechanics*, P. E. Beskos (ed.), V. 3 in *Computational Methods in Mechanics*, North-Holland, Amsterdam, 1987, pp. 333-365.

20. M. Bonnet and H. D. Bui, 'Regular B.I.E. for 3-D cracks in elastodynamics', in: *Advanced Boundary Element Methods*, T. A. Cruse (Ed.), Springer-Verlag, New York, 1987, pp. 41–47.
21. V. A. Kozlov, V. G. Maz'ya and V. Z. Parton, 'Asymptotic form of the stress intensity coefficients in quasistatic temperature problems for a domain with a cut', *PMM (USSR)*, **49**, 482–489 (1985).
22. S. Voutsinas and G. Bergeles, 'Numerical calculation of singular integrals appearing in three-dimensional potential flow problems', *Appl. Math. Modell.* **14**, 618–629 (1990).
23. K. Georg, 'Approximation of integrals for boundary element methods', *SIAM J. Sci. Stat. Comput.*, **12**, 444–453 (1991).
24. K.-J. Bathe and E. L. Wilson, *Numerical Methods in Finite Element Analysis*, Prentice-Hall, Englewood Cliffs, NJ, 1976, Chap. 4.
25. M. H. Aliabadi and W. S. Hall, 'Nonisoparametric formulations for the three-dimensional boundary element method', *Eng. Anal.*, **5**, 198–204 (1985).
26. O. A. Ladyzhenskaya, *The Mathematical Theory of Viscous Incompressible Flow*, Gordon and Breach, New York, 1963.
27. A. Deb and P. K. Banerjee, 'A comparison between isoparametric Lagrangian elements in 2D boundary element method', *Int. j. numer. methods eng.* **28**, 1539–1555 (1989).
28. W. L. Wendland, 'Asymptotic accuracy and convergence for point collocation methods', in C. A. Brabbia (ed.), *Boundary Element Research, Vol. 2*, Springer, New York 1985, pp. 230–257.
29. W. L. Wendland, 'Mathematical properties and asymptotic error estimates for elliptic boundary element methods', in T. A. Cruse (ed.), *Advanced Boundary Element Methods*, Springer, New York 1987, pp. 475–489.
30. D. W. Kelley, R. J. Mills, J. A. Reizes and A. D. Miller, 'A posteriori estimates of the solution caused by discretization in finite element, finite difference and boundary element methods', *Int. j. numer. methods eng.*, **24**, 1921–1939 (1987).
31. C. Y. Chan, 'Hydrodynamic interactions in large aspect ratio fiber suspensions', *Ph.D. Thesis*, University of Delaware, December 1991.
32. A. H. Stroud and D. Secrest, *Gaussian Quadrature Formula*, Prentice-Hall, Englewood Cliffs, NJ, 1966.
33. C. Y. Chan, A. N. Beris and S. G. Advani, 'Use of boundary element method to simulate hydrodynamic interactions around ellipsoids in 3-D flow fields', *Ann. Polymer Processing Society Meeting*, H. H. Winter and M. F. Malone (eds.), University of Massachusetts, Amherst, MA, 4D-4E, August 1989.
34. C. Y. Chan, A. N. Beris and S. G. Advani, 'Simulation of 3-D hydrodynamic interactions around ellipsoidal particles using high order boundary element techniques', in S. Grilli, C. A. Brebbia and A. H.-D. Cheng (eds), *Proc. Fifth Int. Conf. on Boundary Element Technology*, Springer, New York, 1990, pp. 231–252.
35. J. Happel and H. Brenner, *Low Reynolds Number Hydrodynamics*, Martinus Nijhoff, Dordrecht, 1970.
36. S. Kim and R. T. Muffin, 'The resistance and mobility functions of two equal spheres in low-Reynolds-number flow', *Phys. Fluids*, **28**, 2033–2045 (1985).
37. S. Kim, 'Stokes flow past three spheres: an analytic solution', *Phys. Fluids*, **30**, 2309–2314 (1987).
38. S. Kim, 'Sedimentation of 2 arbitrarily oriented spheroids in a viscous fluid', *Int. J. Multiphase Flow*, **5**, 699–712 (1985).
39. A. J. Goldman, G. Cox and H. Brenner, 'Low Reynolds number fluid-particle dynamics I. Motion of two spherical particles in a direction perpendicular to their line of centers', *Chem. Eng. Sci.*, **21**, 1151 (1966).
40. C. M. Bender and S. A. Orszag, *Advanced Mathematical Methods for Scientists and Engineers*, McGraw-Hill, New York, 1978.
41. B. J. Yoon and S. Kim, 'A boundary collocation method for the motion of two spheroids in Stokes flow: hydrodynamic and colloidal interactions', *Int. J. Multiphase Flow*, **16**, 639–649 (1990).
42. R. G. Cox, 'The motion of suspended particles almost in contact', *Int. J. Multiphase Flow*, **1**, 343–371 (1974).
43. S. Kim, personal communication to A.N.B. 13 May 1991.